PNAS
www.pnas.org

Supplementary Information for

Molecular engineering of an efficient four-domain DAF-MCP chimera reveals the presence of functional modularity in RCA proteins

Hemendra Singh Panwar, Hina Ojha, Payel Ghosh, Sagar H. Barage, Sunil Raut, and Arvind Sahu

Corresponding author: Dr. Arvind Sahu, E-mail: arvindsahu@nccs.res.in

This PDF file includes:

Supplementary text (SI Materials and Methods)

Supplementary Tables (S1-S3)

Supplementary Figures (Figs. S1-S10)

References

www.pnas.org/cgi/doi/10.1073/pnas.1818573116

I. SI Materials and Methods

Construction of DAF, MCP, DAF-MCP chimeras and substitution mutants of D2D3M3M4 and CR1 LHR-A (CCP1-3)

Human DAF (D1-D4) and MCP (M1-M4) were amplified from their respective cDNAs and cloned into the yeast expression vector pPICZα (Invitrogen, Carlsbad, CA) as well as the bacterial expression vector pET-28b. The DAF-MCP chimeras were constructed using the gene splicing and overlap extension method as described (1) and then cloned either into the yeast expression vector pPICZα or into the bacterial expression vector pET-28b. The CR1 LHR-A (CCP1-3) was amplified from CR1 cDNA and cloned in the pET-28b for its expression. The primer sets used to amplify the required regions of DAF, MCP and CR1 are listed in **Table S3**. The substitution mutants of D2D3M3M4 and CR1 LHR-A (CCP1-3) were constructed using the Quick-change site-directed mutagenesis kit II (Stratagene, La Jolla, CA) and cloned into the bacterial expression vector pET-28b. The mutagenic primers utilized for the site-directed mutagenesis are listed in **Table S3**. The DAF deletion mutant D2-D3 was amplified from DAF cDNA and cloned into pET-28b; primer sets used are listed in **Table S3**. Following cloning, all the constructs were validated by DNA sequencing (1st Base Laboratories Sdn Bhd, Malaysia). For expression, the proteins/mutants cloned into pPICZα were integrated into *Pichia pastoris* as per the manufacturer's protocol, whereas those cloned into pET-28b were transformed into *Escherichia coli* BL21 (DE3) cells.

Expression and purification of DAF, MCP, DAF-MCP chimeras and substitution mutants of D2D3M3M4

Human DAF, MCP and the DAF-MCP chimeras namely D2M2-4 (chimera containing the DAF linker between D2-D3) and D2M2-4-ML (chimera containing the linker between M1-M2) were expressed in *P. pastoris* as described (2, 3) and purified as below. Firstly, all the expressed proteins were concentrated by ultrafiltration and precipitated using 80% ammonium sulphate on ice. The pellets obtained were then dissolved in PBS and processed further. For purification of DAF, the pellet dissolved in PBS was mixed with 500 mM NaCl and loaded onto a DEAE-Sephacel column (Sigma, St. Louis, Mo.) pre-equilibrated with PBS containing 500 mM NaCl. The flow-through obtained was then passed through a PD-10 column (GE Healthcare Life Sciences, Pittsburgh, PA) for buffer exchange and loaded onto a Mono Q column in 20 mM Tris, pH 8.0. Elution of the bound DAF was achieved by passing a linear gradient of 0 to 500 mM NaCl. For purification of MCP and the chimeras (D2M2-4-DL and D2M2-4-ML), the pellet dissolved in PBS was subjected to buffer exchange against 10 mM sodium phosphate, pH 7.4 and loaded onto a DEAE-Sephacel column in the same buffer. The bound proteins were eluted with a linear gradient of 0-500 mM NaCl. The fractions containing MCP or the respective chimera were pooled, exchanged into 20 mM Tris, pH 8.0, loaded onto Mono Q column and eluted with a linear gradient of 0-500 mM NaCl. Eluted fractions in all the above purifications were subjected to SDS-PAGE and Western blot analysis using the appropriate antibody. All the purified proteins were dialyzed

in PBS and concentrated by ultrafiltration; purity of all the proteins exceeded 95% as determined by SDS-PAGE (**Figs. S10A and S10B**).

Human DAF and MCP were also expressed in *E. coli*. Other mutants that were expressed in *E. coli* include the DAF mutant D2D3, DAF-MCP chimeras D2D3M3M4 and D2D3D4M4, and substitution mutants of D2D3M3M4. The CR1 LHR-A (CCP1-3) and its mutant CR1 LHR-A^{mut} (CCP1-3, D109N/E116K) were also expressed in *E. coli*. Expression of these proteins was performed essentially as described earlier (4, 5). In brief, proteins were purified using Ni-NTA column in the presence of urea as they were present in the inclusion bodies. They were then subjected to refolding by rapid dilution method (3) and passed through gel filtration column (Superose 12; GE Healthcare Life Sciences). All the proteins refolded properly as judged by the presence of a monodisperse population in the size exclusion chromatography profiles, and mobility differences on SDS-PAGE under reducing and non-reducing conditions (an indication of disulfide bond formation) (**Figs. S10A and S10B**). The purity of all the *E. coli* expressed proteins exceeded 95% as determined by SDS-PAGE.

CP and AP C3-convertase decay-accelerating activity assay

The classical/lectin and alternative pathway C3-convertase decay-accelerating activity of DAF, DAF-MCP chimeras and the mutants of D2D3M3M4 was measured using hemolytic assays as described (2, 6). Briefly, the respective convertases were formed on erythrocytes using purified complement components and allowed to decay in the presence or absence of a regulator. The activity of the remaining convertases was estimated by incubating the erythrocytes with guinea pig sera containing 40 mM EDTA (a source of C3-C9) and measuring lysis. The data obtained were normalized by considering 100% C3-convertase activity equal to the lysis that occurred in the absence of an inhibitor. The activity obtained was then plotted against the concentration to determine the inhibitor concentration required to inhibit 50% of enzyme activity (IC_{50}). Each of the inhibitors was tested at various concentrations to determine the concentration range at which it inhibits and then it was tested at three specific concentrations to determine the IC_{50} as performed earlier (7-10).

C3b and C4b cofactor activity assay

The cofactor activity of MCP, DAF-MCP chimeras and the mutants of D2D3M3M4 was measured by incubating each of the regulator with C3b (purified as described (11)) or C4b (Complement Technology, Inc., Tyler, TX) and serine protease factor I in PBS and measuring C3b/C4b cleavage. Briefly, C3b (10 µg) or C4b (15 µg) was mixed with 1 µM (for C3b) or 2 µM (for C4b) of the regulator and 250 ng (for C3b) or 500 ng (for C4b) of factor I in a total reaction volume of 75µl and incubated at 37^{O}C. Aliquots of 15µl were then taken out at the indicated time periods, mixed with the sample buffer containing DTT and ran on either 9% (for C3b) or 10% (for C4b) SDS-PAGE gels for determining cleavage of α'-chain of C3b/C4b. The percentage of α'-chain cleaved was calculated by densitometric analysis using the Quantity one software (*Bio-Rad*); the amount of α'-chain was normalized to β-chain (loading control). A plot of percent cleavage of the α'-chain of C3b/C4b against time

provided the 50% cleavage of α'-chain of C3b/C4b. Activity differences of ≥3-fold were considered significant (12, 13).

Surface plasmon resonance measurements

Binding measurements of DAF, MCP, DAF-MCP chimeras and substitution mutants of D2D3M3M4 to C3b and C4b were performed on Biacore 2000 (Biacore AB, Uppsala, Sweden). First, the target proteins C3b and C4b biotinylated at their free –SH groups using EZ-Link PEO-maleimide-activated biotin (Pierce, Rockford, IL), were immobilized on flow cells 2 and 3 of a streptavidin chip (Sensor Chip SA; Biacore AB). The flow cell-1 immobilized with biotinylated bovine serum albumin (BSA) served as the control flow cell. Next, each of the analytes (DAF, MCP and DAF-MCP chimeras and the mutants of D2D3M3M4) in PBS-T was flowed over the chip at 50 µl/min at 25^{O}C to measure binding. The association and dissociation of the analyte was measured for 120 and 180 s, respectively, and chip regeneration was achieved by 30s pulses of 0.2 M sodium carbonate, pH 9.5. The specific binding response was derived by subtracting the control flow cell data from the target protein immobilized flow cell data.

ELISA for measurement of effect on CP, AP and LP

We employed the Wieslab complement system screen ELISA assay (Euro-Diagnostica, Malmo, Sweden) to test the relative complement pathway-specific inhibitory activity of the multi-5 mutant with that of MCP, DAF, CR1 LHR-A (CCP1-3) and CR1 LHR-A^{mut} (CCP1-3, D109N/E116K). Herein, the graded concentrations of each of the test proteins were made in the pathway-specific diluent and mixed with a fixed percentage of normal human serum concentration as detailed in the manual. The reaction mixtures (100 µl) were then added to the microtiter wells coated with pathway-specific activators and kept for 60 min at 37^{O}C. Thereafter, wells were washed three times with the washing solution supplied in the kit and incubated for 30 min at room temperature with an antibody against C5b-9 (100µl) labelled with alkaline-phosphatase. The wells were again washed three times with the washing solution and incubated for 30 min at room temperature with the substrate (100µl). The absorbance was read at 405 nm on a microplate reader. The level of serum activity in the presence of regulatory proteins was expressed as percent of activity measured without the proteins.

Modelling of D2D3M3M4 chimera

The sequence of DAF (UniProt ID: P08174) and MCP (UniProt ID: P15529) were retrieved from the UniProt Protein sequence database. The sequence of D2D3 extracted from DAF and M3M4 from MCP to construct chimera sequence. The structural co-ordinates of DAF and MCP were separated from co-crystal structures of C3b-DAF (PDB id: 5FOA) and C3b-MCP (PDB id: 5FO8) respectively. We modelled the structure of chimera (D2D3M3M4) based on DAF and MCP template structures using Modeller 9.11 (14) implemented in Discovery Studio v 3.5 ((15); Dassault Systèmes BIOVIA 2016). Subsequently, a loop modelling option was used to model the loop regions. The single best model was selected on the basis of the

DOPE score. The stereochemical quality of the predicted model was evaluated using PROCHECK (16) and PROSA-Web servers (17). Then, using Discovery studio, we mutated naturally occurring residues of the chimera with mutant residues (F197I, S199K, P216K, E^{219}CREIY^{224} to I^{219}CEKVL^{224}) derived from experimental evidence as described in the main text. The individual mutant structure of a chimera was then subjected to a calculation of its mutational energy and its stability.

Construction of ternary DAA complex (C3b-D2D3M3M4-Bb) and its interface analysis

The DAA ternary complex with chimera D2D3M3M4 as the regulator was modelled by using the template structures of DAF-C3b (PDB id: 5FOA) and C3bBb (PDB id: 2WIN) along with the above-modelled structure of chimera D2D3M3M4. Briefly, the D2D3M3M4 chimera was superimposed to DAF in the C3b-DAF structure to make the D2D3M3M4-C3b complex. The D2D3M3M4-C3b and C3bBb were then superimposed together with reference to C3b molecule to generate a ternary model of C3b-D2D3M3M4-Bb. The final ternary complex was subjected to energy minimisation by the steepest descent method. The interface analysis of the ternary complex was performed by PISA (Protein interface analysis program, www.ebi.ac.uk/msd-srv/prot_int/pistart.html) to understand the interaction between C3b and D2D3M3M4 as well as Bb and D2D3M3M4.

Construction of ternary complex (C3b-multi-4 mutant-FI) and MD simulation

The ternary complex of C3b-FH-FI (PDB id: 5O32) was retrieved from PDB and the model of the multi-4 mutant was superimposed against the FH molecule of the complex. The coordinates of FH were removed and a ternary complex of C3b-multi-4 mutant-FI was generated using UCSF Chimera (18). The generated ternary complex of C3b-multi-4 mutant-FI was then subjected to MD simulation with OPLS-AA force field using the GROMACS 5.0.4 package (19, 20). The protein was solvated with simple point charge (SPC) water model and neutralized with NA+ counter ions. The solvated structure was minimized by steepest descent energy minimization followed by 500 ps equilibration in NVT ensemble with position restraints applied to protein. Subsequently, the system was equilibrated for 2 ns using NPT ensemble. Finally, each ternary complex system was subjected to 50 ns MD simulation in the NPT ensemble. A time step of 2 fs was used throughout simulation with periodic boundary conditions. The LINCS algorithm (21) was used to restrain all bonds to the hydrogen atom, permitting a time step of 2 fs. The long-range electrostatic interactions were calculated using the PME algorithm with a cutoff distance 1.2 nm (22). Structural clustering was performed on the whole trajectory with RMSD cutoff 2.0 Å using g_cluster tool implemented in GROMACS (23). The single representative conformation was extracted from the highest populated cluster of each system. The trajectory was analysed using VMD and simulation images were generated using Discovery Studio ((15); Dassault Systèmes BIOVIA 2016).

II. SI Tables

Table S1: Summary of the complement regulatory activities of DAF, MCP and various DAF-MCP chimeric mutants

	C3b CFA		C4b CFA		AP-DAA		CP-DAA	
Wild type /Mutant	**Time (min.) for 50% cleavage of C3b α'-chain**	**Relative C3b CFA**	**Time (min.) for 50% cleavage of C4b α'-chain**	**Relative C4b CFA**	**DAA IC50 (nM)**	**Relative AP-DAA**	**DAA IC50 (nM)**	**Relative CP-DAA**
a. DAF-MCP chimeras								
DAF	NA	NA	NA	NA	1.1 ± 0.3	1	14.5 ± 6.5	1
MCP	3.5 ± 1.7	-	16.5 ± 4.9	-	NA	NA	NA	NA
D2M2-4	ND	ND	ND	ND	> 10	< 0.1	456.7 ± 60.3	0.03
D2M2-4 (MCP linker)	ND	ND	ND	ND	> 10	< 0.1	> 1000	< 0.01
DAF	NA	NA	NA	NA	2.3 ± 1.6	1	2.6 ± 2.6	1
MCP	2.1 ± 0.2	1	12 ± 6.8	1	NA	NA	NA	NA
D2D3M3M4	80.7 ± 2.5	34	428.6 ± 77.8	35	2.4 ± 1.6	1	5.1 ± 4.5	0.5
D2D3D4M4	ND	ND	ND	ND	5.6 ± 3.2	0.4	5.7 ± 8.8	0.4
D2D3	ND	ND	ND	ND	> 10	< 0.2	10.9 ± 4.7	< 0.3
b. Gain-of-function mutants of D2D3M3M4								
D2D3M3M4	82.6 ± 4.6	1	464.7 ± 65.4	1	2.1 ± 0.30	1	15.9 ± 6.7	1
T192E	74.3 ± 22.3	1.1	268 ± 61.6	1.7	2.3 ± 0.3	0.9	15.3 ± 6.7	1
K195Y	complete loss	complete loss	> 540	< 0.85	> 10	**0.2**	> 100	**0.2**
F197I	49.8 ± 5.2	1.7	**66.7 ± 22**	**7**	4.4 ± 1.6	0.5	30.7 ± 8.0	0.5
S199K	18.9 ± 2.6	**4.4**	**181.3 ± 37.1**	**2.5**	6.6 ± 2.3	0.3	21.7 ± 14.2	0.7
T200Y	103.3 ± 11.0	0.8	513.3 ± 46.2	0.9	3.7 ± 0.20	0.56	17.7 ± 6.4	0.9
L205K	103.6 ± 10.2	0.8	433.3 ± 94.5	1.07	> 10	**0.2**	9.2 ± 5.8	1.7
P216K	30.1 ± 4.1	**2.7**	**93.3 ± 15.2**	**5**	3.4 ± 0.5	0.6	21 ± 12	0.75
multi-1	27.3 ± 3.2	**3**	433.3 ± 117.1	1.07	1.9 ± 0.6	1.1	22.6 ± 10.2	0.7
multi-2	4.3 ± 0.52	**19.2**	**44.3 ± 17**	**10.5**	> 10	**0.2**	5.8 ± 3.3	2.7
multi-3	3.8 ± 2.1	**22**	**16.7 ± 0.6**	**28**	8.5 ± 1.6	**0.24**	12.3 ± 7.2	1.3
c. Multi mutants of D2D3M3M4								
MCP	4.5 ± 0.5	1	9.3 ± 1.2	1	NA	NA	NA	NA
multi-4	17.5 ± 5.5	0.25	5.5 ± 2.0	1.7	> 10	< 0.3	39.3 ± 7.8	0.4
multi-5	3.3 ± 0.5	1.3	3.1 ± 0.3	**3**	2.4 ± 0.4	1.3	12.7 ± 6.5	1.3
DAF	NA	NA	NA	NA	3.1 ± 0.8	1	16.5 ± 8.7	1

Boldface indicates the mutants and data with a > 3-fold difference in activity, which was considered significant. NA – No activity, ND- not determined. Data are reported as mean ± SD of three independent experiments. Multi-1 (linker substitution ; 219ECREIY224 to ICEKVL), multi-2 (linker substitution + S199K) and multi-3 (215DPL217 to PKA), multi-4 (linker substitution + S199K + P216K + F197I), multi-5 (linker substitution + P216K + F197I)

Table S2: Comparison of complement regulatory activities of multi-5 (DCP) with DAF, MCP, LHR-A (CCP1-3), LHR-A (CCP1-3, D109N/E116K).

Table S2A:

	Total pathway inhibitory activity					
Wild type /Mutant	**Inhibition of AP activity IC_{50} (μM)**	**Relative AP activity**	**Inhibition of LP activity IC_{50} (μM)**	**Relative LP activity**	**Inhibition of CP activity IC_{50} (μM)**	**Relative CP activity**
1. DAF	0.3 ± 0.2	1	0.11 ± 0.07	1	0.05 ± 0.02	1
2. MCP	1.4 ± 0.4	0.21	2.0 ± 0.3	0.05	> 2.25	< 0.02
3. multi-5 (DCP)	0.04 ± 0.01	**7.5**	0.05 ± 0.02	**2.2**	0.01 ± 0.02	**5**

Table S2B:

	Total pathway inhibitory activity					
Wild type/Mutant	**Inhibition of AP activity IC_{50} (μM)**	**Relative AP activity**	**Inhibition of LP activity IC_{50} (μM)**	**Relative LP activity**	**Inhibition of CP activity IC_{50} (μM)**	**Relative CP activity**
1. CR1 LHR-A (CCP1-3)	0.64 ± 0.09	1	0.08 ± 0.04	1	0.06 ± 0.02	1
2. CR1 LHR-A^{mut} (CCP1-3, D109N/E116K)	0.17 ± 0.02	**3.8**	0.015 ± 0.002	**5.3**	0.02 ± 0.005	**3**
3. multi-5 (DCP)	0.06 ± 0.008	**10.6**	0.02 ± 0.004	**4**	0.04 ± 0.02	1.5

Boldface indicates the mutants and data with a >2-fold difference in activity, which was considered significant. Data are reported as mean ± SD of three independent experiments. AP, alternative pathway; CP, classical pathway; LP, lectin pathway.

Table S3: Primers used for the cloning of wild-type DAF, MCP and DAF-MCP region swap mutants

Wild type/Mutant[a]	Amplified product[b]	Primer	Sequence[c]
DAF-pichia	D1-D4	Forward	ggAATTCgACTGTggCCTTCCCCCAgATg
DAF-pichia	D1-D4	Reverse	gCTCTAgA TTATCTgCATTCAggTggTgggCC
DAF	D1-D4	Forward	ggAATTCCATATggACTgTggCCTTCCCCCAgATg
DAF	D1-D4	Reverse	CCgCTCgAgTCTgCATTCAggTggTgggCCAC
MCP-pichia	M1-M4	Forward	ggAATTCgCCTgTgAggAgCCACCAAC
MCP-pichia	M1-M4	Reverse	gCTCTAgATTAAAgACACTTTggAACTggggg
MCP	M1-M4	Forward	CATgCCATgggCAAgTgTgAggAgCCACCAACATTTgAAgCTATggAgCTCATTggTAAACCAAAACCC
MCP	M1-M4	Reverse	CGCAAGCTTAAGACACTTTGGAACTGGG
D2D3	D2D3	Forward	CCCAAgCTTgCgAggTgCCAACAAggCTAAATTC
	D2D3	Reverse	CCgCTCgAgATAAATTTCTCTgCACTCTggCAACgg
D2M2-4	D2	Forward	ggAATTCTgCgAggTgCCAACAAggC
	D2	Reverse	**CCCgTATATATggACATgATTTCTTTTTACAAAATTCg**ACTg
	M2M3M4	Forward	**CgAATTTTgTAAAAAgAAATCATgTCCATATATACggg**ATCCTTTAAATgg
	M2M3M4	Reverse	gCTCTAgAgCAAgACACTTTggAACTggggg
D2M2-4 (ML)	D2(ML)	Forward	ggAATTCTgCgAggTgCCAACAAggC
	D2(ML)	Reverse	**ggACATgTTTCTCTATAACAAAATTCgACTgCTg**TggACC
	M2M3M4	Forward	**CAgCAgTCgAATTTTgTTATAgAgAAACATgTCC**ATATATACg
	M2M3M4	Reverse	gCTCTAgAgCAAgACACTTTggAACTggggg
D2D3M3M4	D2D3	Forward	CATgCCATgggCTgCgAggTCCCAACAAgg
	D2D3	Reverse	**ggAggTggTgTACAATAAATTTCTCTgCAC**TCTggC
	M3M4	Forward	**gTgCAgAgAAATTTATTgTACACCACCTCC**AAAAATAAAAAATgg
	M3M4	Reverse	CGCAAGCTTAAgACACTTTggAACTggg
D2D3D4M4	D2D3D4	Forward	CATgCCATgggCTgCgAggTCCCAACAAgg
	D2D3D4	Reverse	**gACATTTgACCACTTTgCATTCAggTggTggg**CCAC
	M4(ML)	Forward	**ggACCACCTgAATgCAAAgTggTCAAATgTCg**ATTTCC
	M4(ML)	Reverse	CgCAAgCTTAAgACACTTTggAACTggg
LHR-A^{mut} (CR1CCP1-3 D109N)	-	Forward	CATgCATCATCTCAggT*AAC*ACTgTCATTTgggATAAT
		Reverse	ATTATCCCAAATgACAgT*gTT*ACCTgAgATgATgCATg
LHR-A^{mut} (CR1CCP1-3 E116K)	-	Forward	CTgTCATTTgggATAAT*AAA*ACACCTATTTgTgACAg
		Reverse	CTgTCACAAATAggTgT*TTT*ATTATCCCAAATgACAg

[a] CCP Domains of DAF and MCP are denoted by D and M, respectively, and numbers denote the domain number of the respective regulator.

[b] Restriction sites are underlined. Boldface region indicate the overlapping region of primer with the neighbouring regions/linker at 5' and/or 3' regions. Italics letters represent the mutation

[c] Pichia indicates the proteins were cloned in pPICZA vector. All other proteins were cloned in pET-28b vector.

III. SI Figures

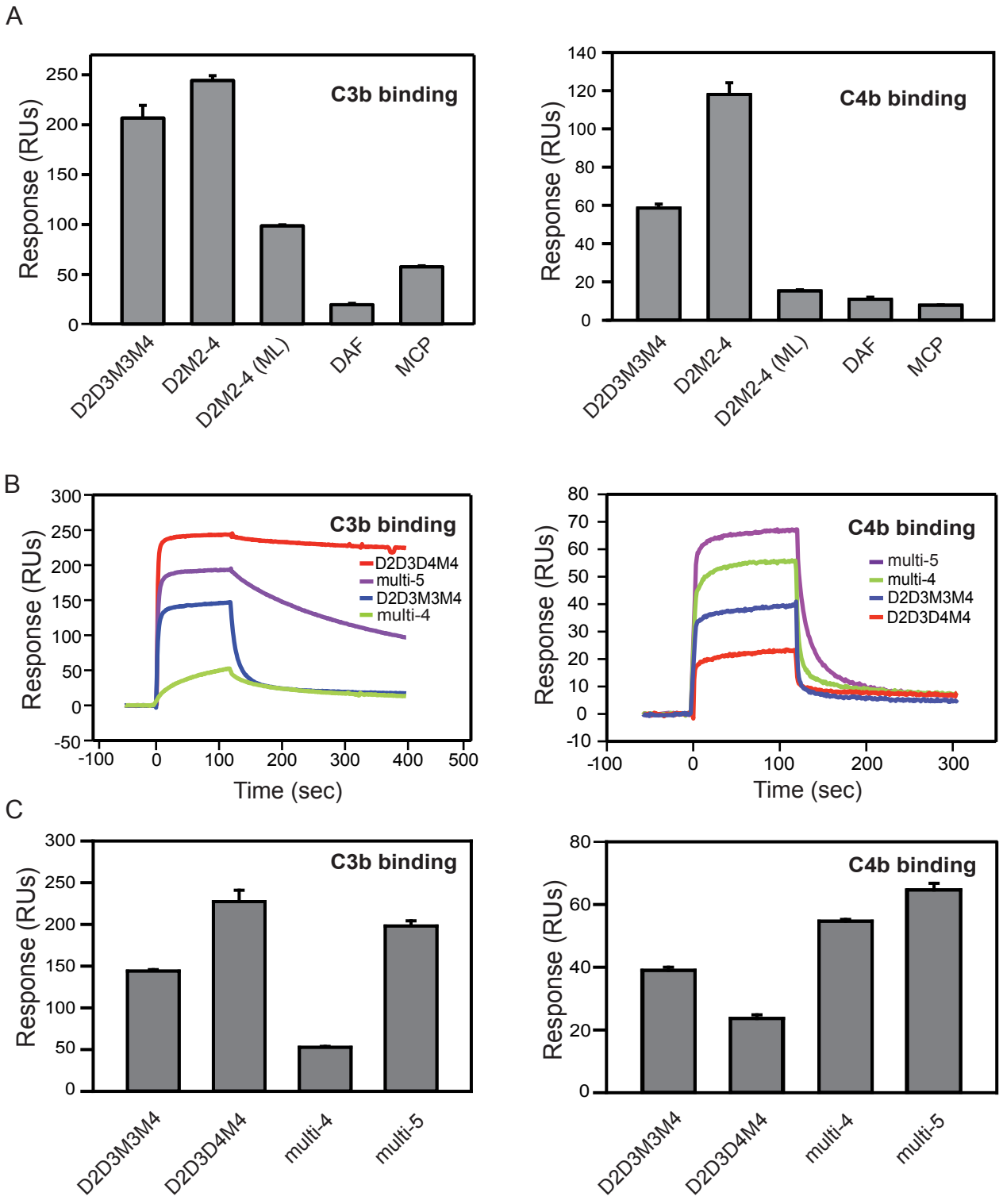

Fig. S1. Binding analysis of DAF, MCP and the DAF-MCP chimeras to C3b and C4b. (A) Relative binding of DAF, MCP and the DAF-MCP chimeras to C3b (left panel) and C4b (right panel). The bar graphs represent RUs achieved at the steady state following binding of the respective protein (1μM) to C3b and C4b. The amount of C3b and C4b-biotin immobilised were 3330 RUs and 1630 RUs, respectively. The data is presented as mean ± SD of three independent experiments. (B) Binding of D2D3M3M4, D2D3D4M4 and the multiresidue mutants of D2D3M3M4 to C3b (left panel) and C4b (right panel). Data shown here is one of the three independent experiments shown in panel C. (C) Relative binding of D2D3M3M4, D2D3D4M4 and the multiresidue mutants of D2D3M3M4 to C3b (left panel) and C4b (right panel). The data is mean ± SD of three independent experiments.

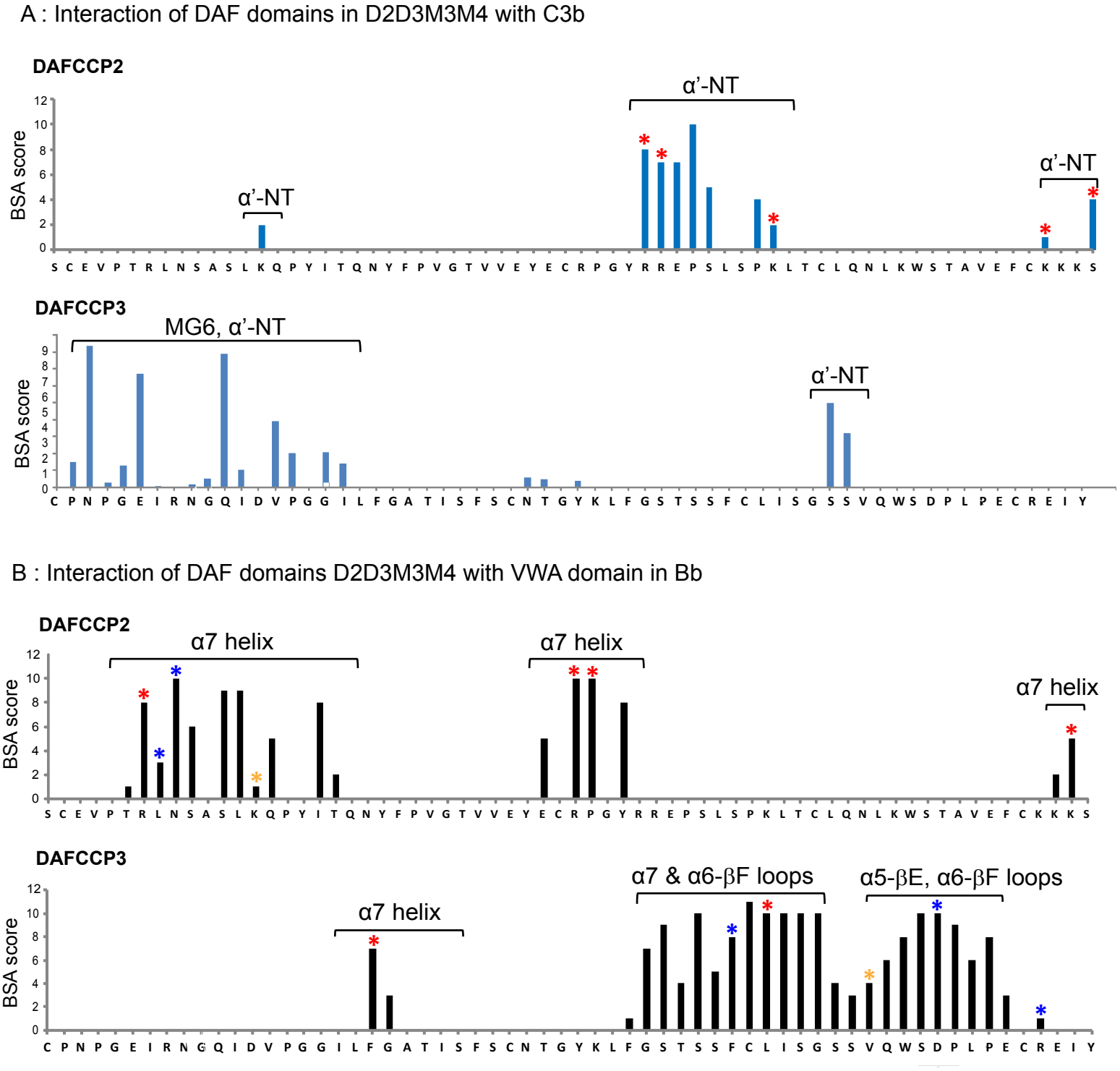

Fig. S2. Interface analysis of the D2D3M3M4 chimera with Bb and C3b in the C3b-D2D3M3M4-Bb complex. The interface of the chimera with C3b and Bb in the modelled structure C3b-D2D3M3M4-Bb complex was analyzed by protein interface analysis program PISA, www.ebi.ac.uk/msd-srv/prot_int/pistart.html. The residues in the D2-D3 domains of D2D3M3M4 chimera that are at the interface of C3b (A) and Bb (B) are shown as vertical bars (which indicates buried surface area (BSA) score) and are colored in blue and black, respectively. The regions of Bb and C3b that interact with these residues of chimera are also marked above the vertical bars. The star marks represent the residues which have been identified earlier by mutagenesis as important for DAA (17). AP-DAA – Blue, CP-DAA –Yellow, both CP and AP-DAA – Red.

A

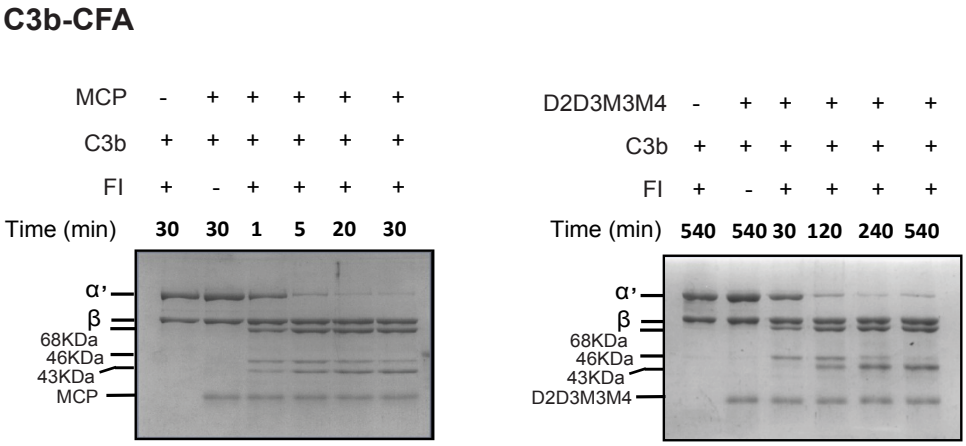

B

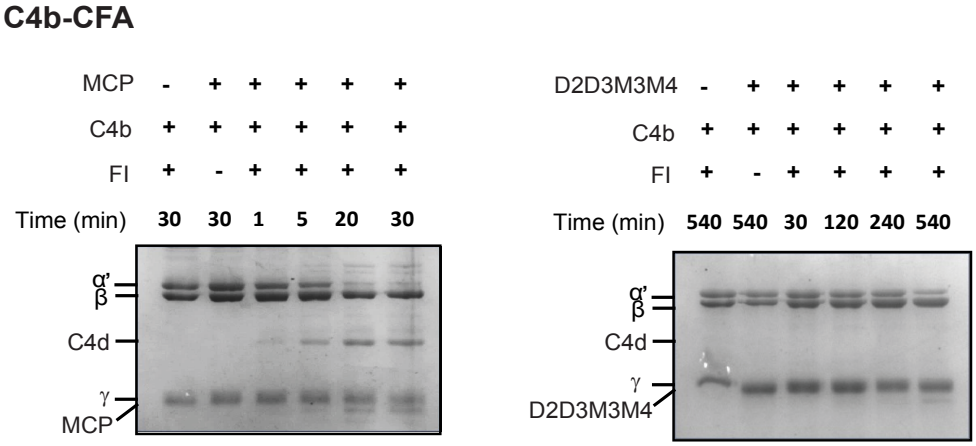

Fig. S3. Cofactor activity measurements of MCP and the DAF-MCP chimera D2D3M3M4. The cofactor activity of these proteins was measured by incubating them with C3b (A) or C4b (B) and factor I at 37ºC for the indicated time in PBS. The cleavage products of C3b/C4b were observed by running them on SDS-PAGE (9% for C3b and 10% for C4b) under reducing conditions. In C3b-CFA, the α'-chain is cleaved into N-terminal 68-kDa and C-terminal 46-kDa fragments amongst which the 46-kDa fragment is further cleaved into 43-kDa fragment. In C4b-CFA, the α'-chain is cleaved into N-terminal 27-kDa, central C4d and C-terminal 16-kDa fragments; the C-terminal fragment is not visualized on the gel.

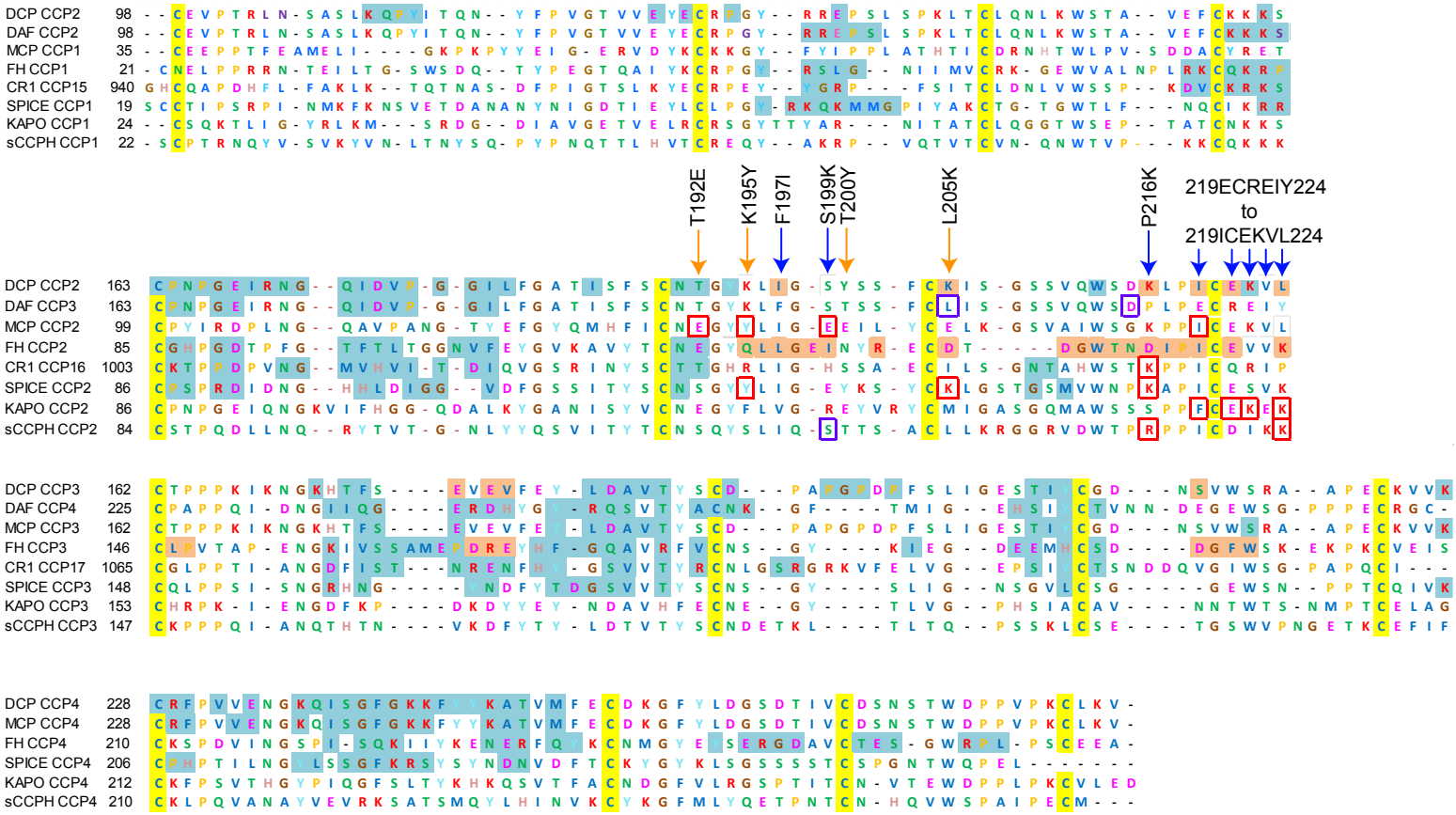

Fig. S4. Structure-based sequence alignment of CCP1-4 of DCP (multi-5 mutant) with homologous domains of various complement regulators. The modelled structure of DCP was aligned with experimental structures of DAF (PDB:1OJV), MCP (PDB:3O8E), Factor H (PDB:2WII), CR1 (PDB:1GKG), and SPICE (PDB:5FOB) , and the modelled structures of Kaposica and CCPH based on CRRY (PDB:2XRB) using the PROMALS3D tool (http://prodata.swmed.edu/promals3d/). Blue arrows indicate the mutations (F197I, S199K, P216K, 219ECREIY224 to ICEKVL) that enhanced CFA in D2D3M3M4 chimera, while orange arrows indicate the mutations (T192E, K195Y, T200Y, L205K) that did not enhance CFA. The highlighted residues indicate interfaces of the respective protein with C3b (light blue) and factor I (light orange). The red boxes indicate previous mutations that resulted in loss in CFA and the violet boxes indicate the mutations that resulted in loss in DAA. The numbering of the domains (shown in the beginning of each CCP sequence) is made according to the uniprot numbering.

Fig. S5A

C3b-CFA

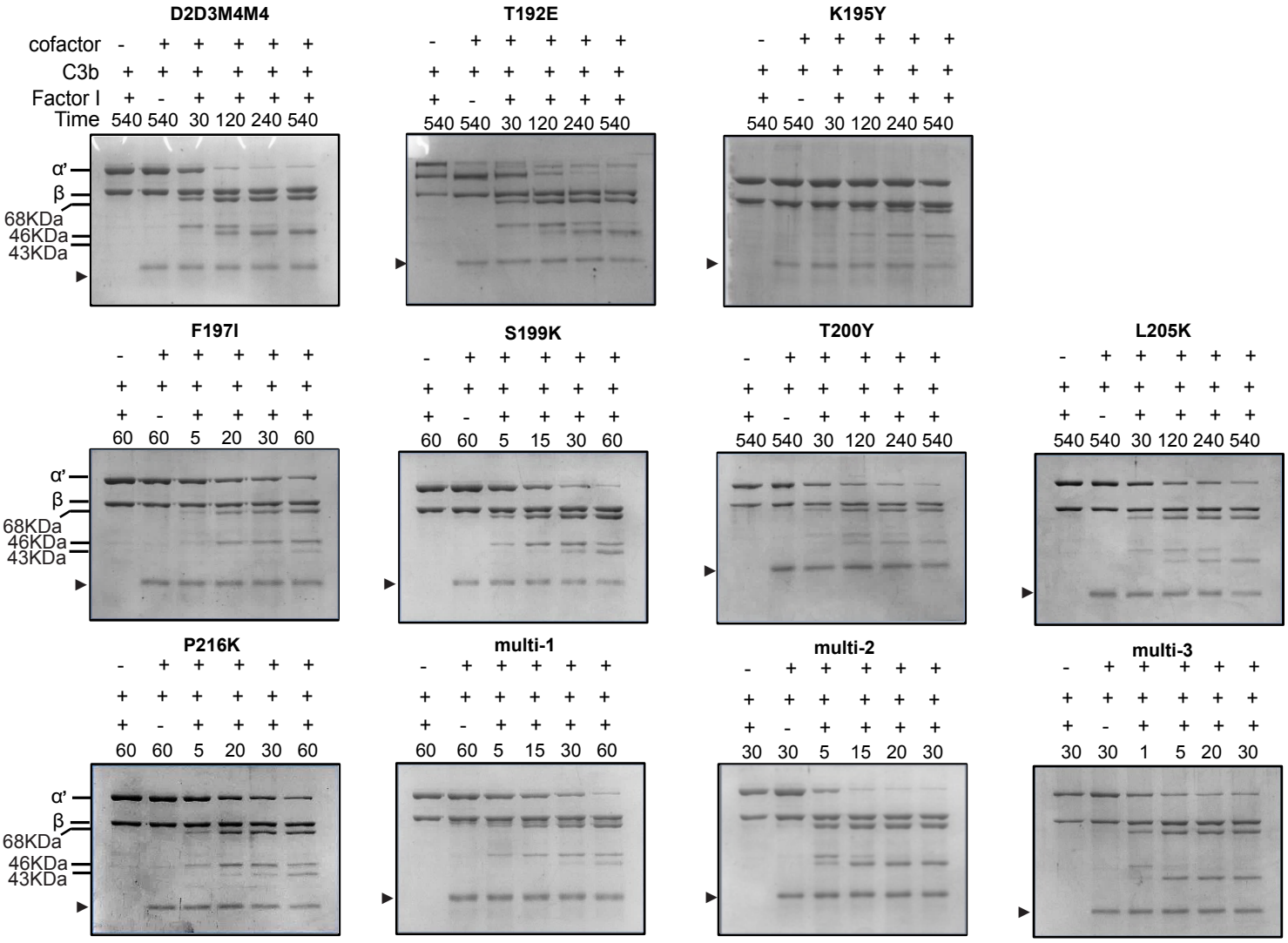

Fig. S5A. Comparison of cofactor activity of the point mutants of D2D3M3M4 with D2D3M3M4. (A) C3b cofactor activity (C3b-CFA) of D2D3M3M4 and the point mutants D2D3M3M4. Arrowheads indicates the cofactor protein/mutant used in the assay.

Fig. S5B

C4b-CFA

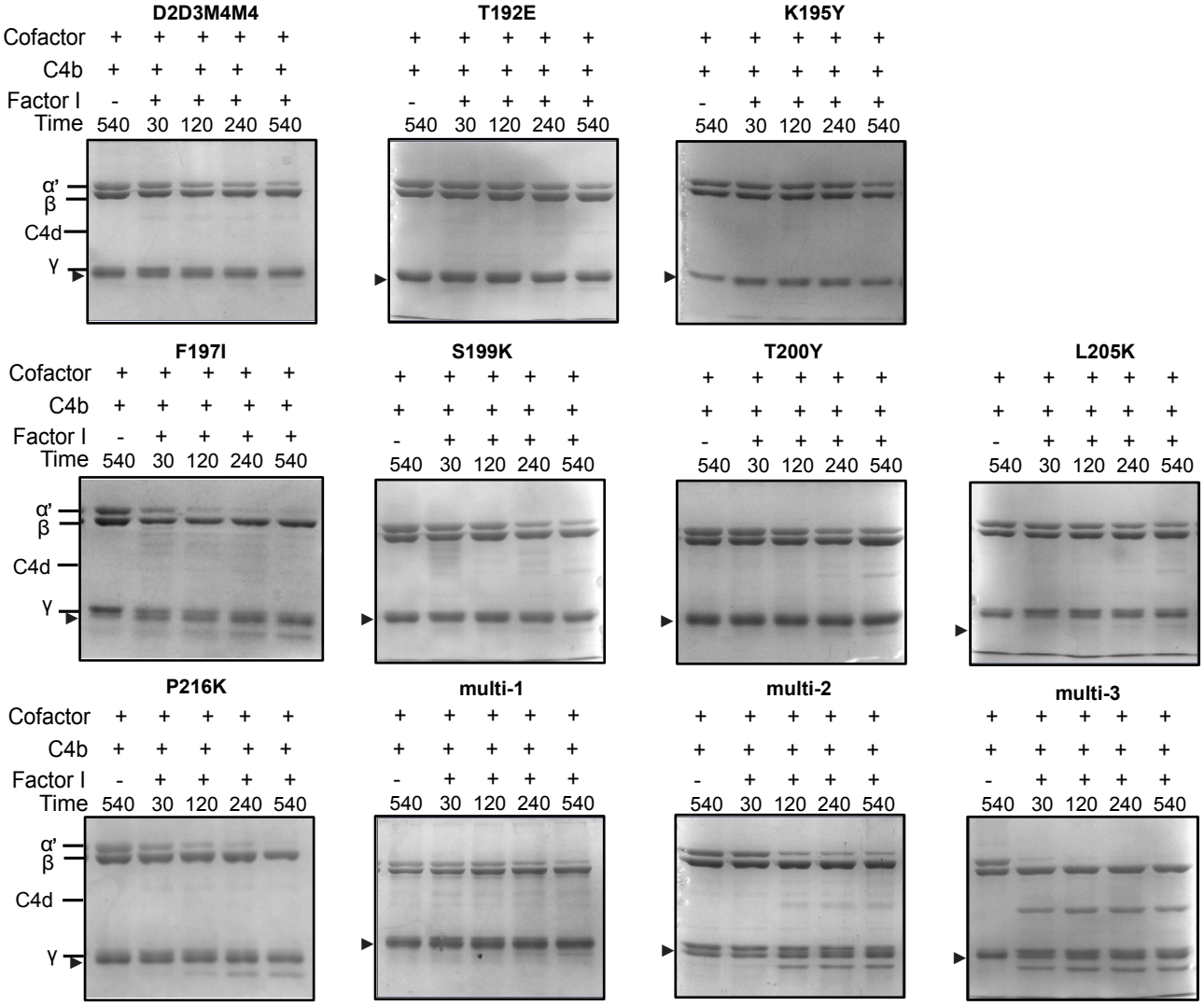

Fig. S5B. Comparison of cofactor activity of the point mutants of D2D3M3M4 with D2D3M3M4 and MCP. (B) C4b cofactor activity (C4b-CFA) of MCP, D2D3M3M4 and the point mutants of D2D3M3M4. Arrowheads indicates the cofactor protein/mutant used in the assay.

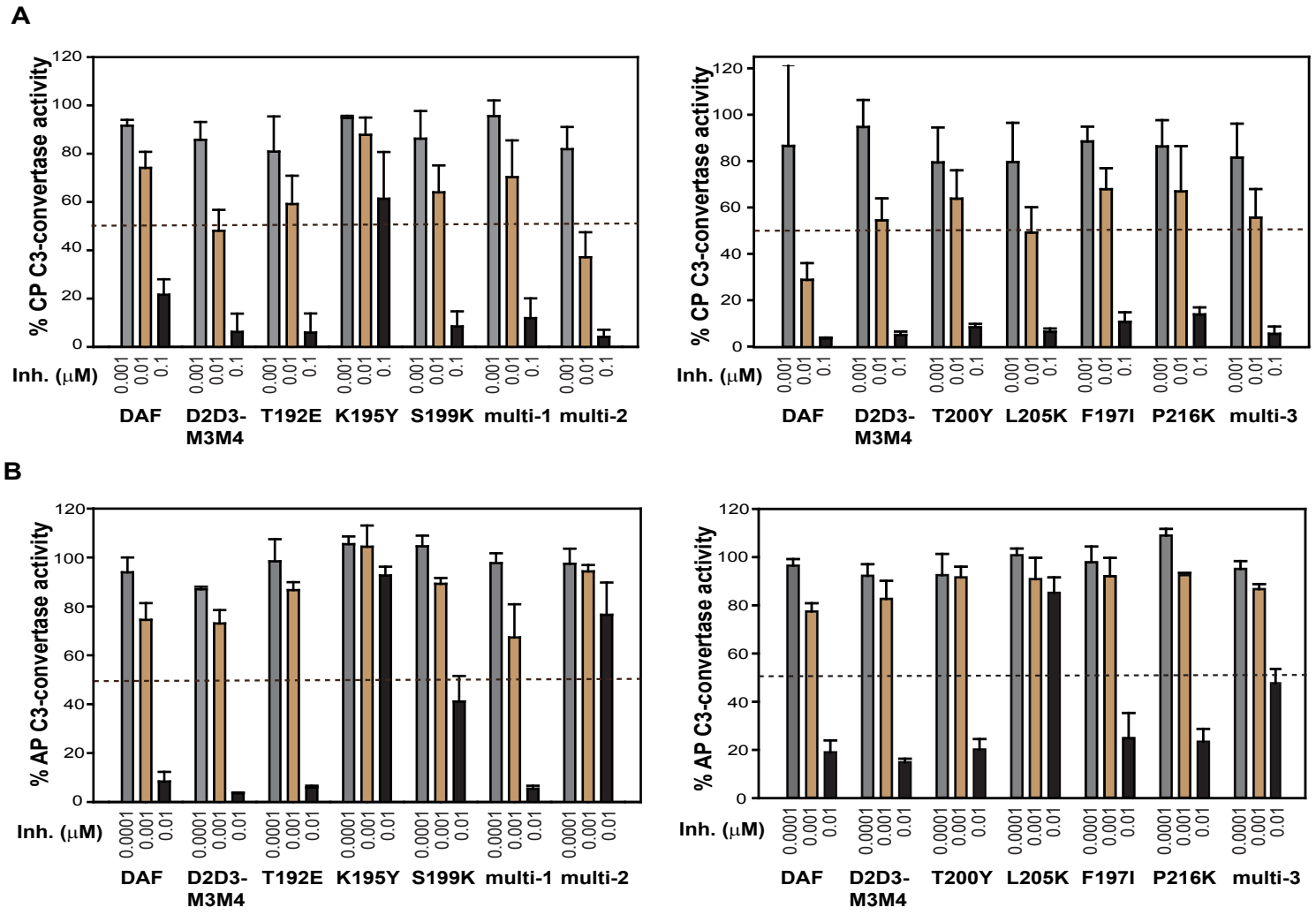

Fig. S6. CP-DAA and AP-DAA measurements of DAF, D2D3M3M4, and the single and multiresidue mutants of D2D3M3M4. (A) CP-DAA of the respective protein was measured by evaluating their ability to decay the pre-formed CP C3-convertase (C4b2a). (B) AP-DAA of the respective proteins was measured by evaluating their ability to decay the pre-formed AP C3-convertase (C3bBb). The data was normalized by considering the 100% C3-convertase activity to be equal to the activity without the inhibitor (Inh.). Data shown are mean ± SD of three independent experiments.

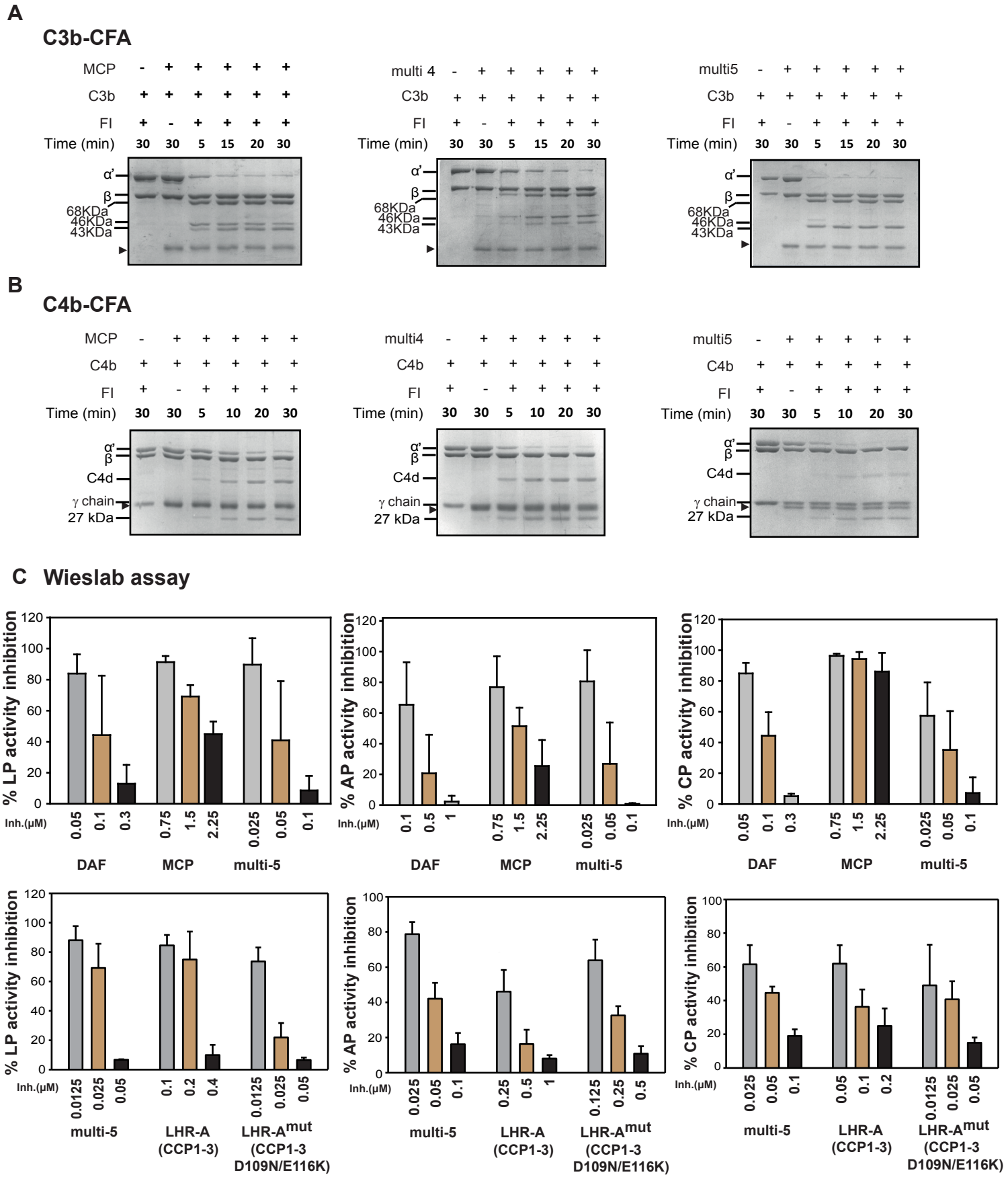

Fig. S7. Comparison of cofactor activity of the multi-residue mutants of D2D3M3M4 with MCP. (A) C3b cofactor activity (C3b-CFA) of MCP, multi-4 and multi-5. (B) C4b cofactor activity (C4b-CFA) of MCP, multi-4 and multi-5. Arrowheads indicates the cofactor protein/mutant used in the assay. (C) Relative effect of DAF, MCP, CR1 LHR-A (CCP1-3), CR1 LHR-A (CCP1-3 D109N/E116K) and the D2D3M3M4 mutant multi-5 on the classical, alternative and lectin pathways. The relative effect of the indicated proteins was measured by employing Wieslab total complement ELISA kit. Data are mean ± SD of three independent experiments.

Fig. S8A

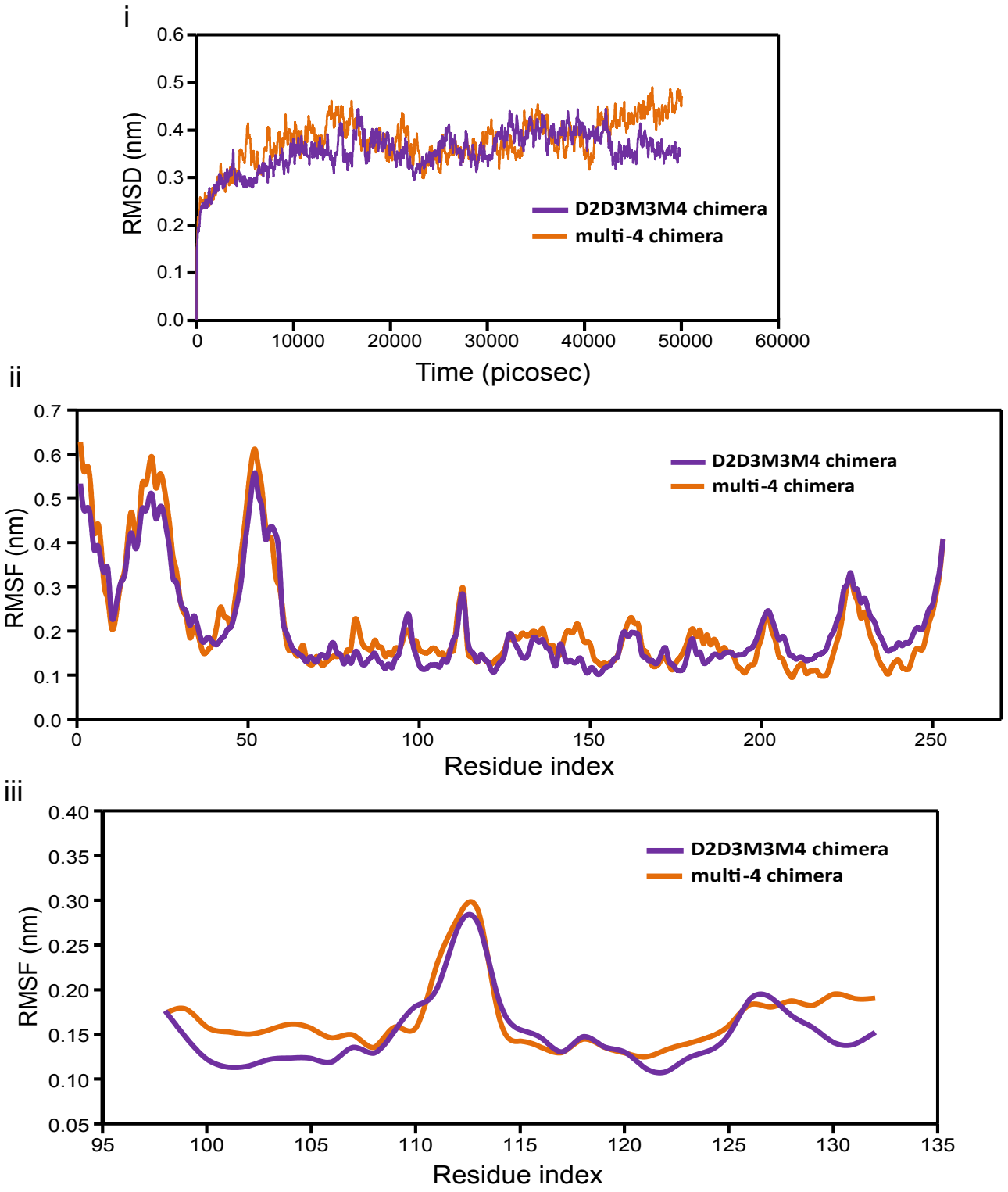

Fig. S8A. RMSD and RMSF plots of C3b-multi4-FI complex. (i) Backbone RMSD of C3b-multi4-FI complex for 50ns simulation. (ii) Root mean square fluctuation (RMSF) of chimera residues for the entire simulation time. (iii) Plot showing the RMSF of the multi-4 mutant residues located in the region where gain-of-function mutations have been identified.

Fig. S8B

i

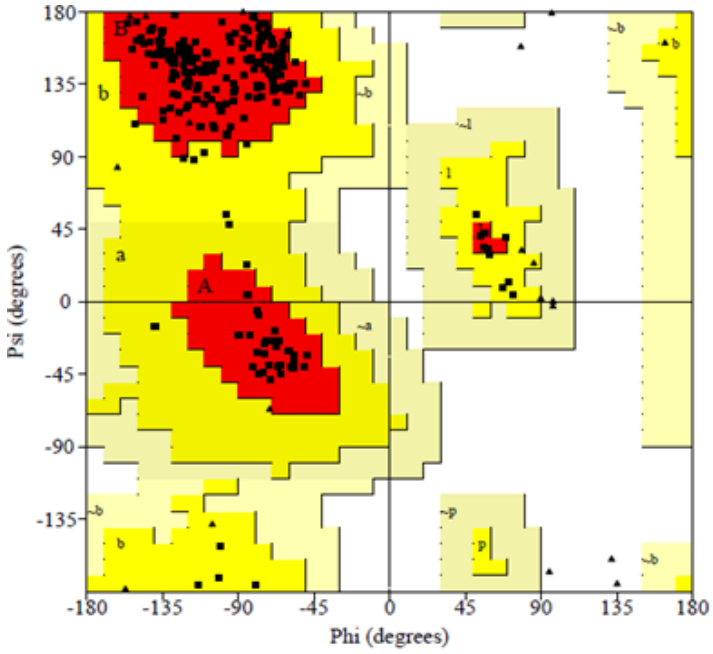

ii

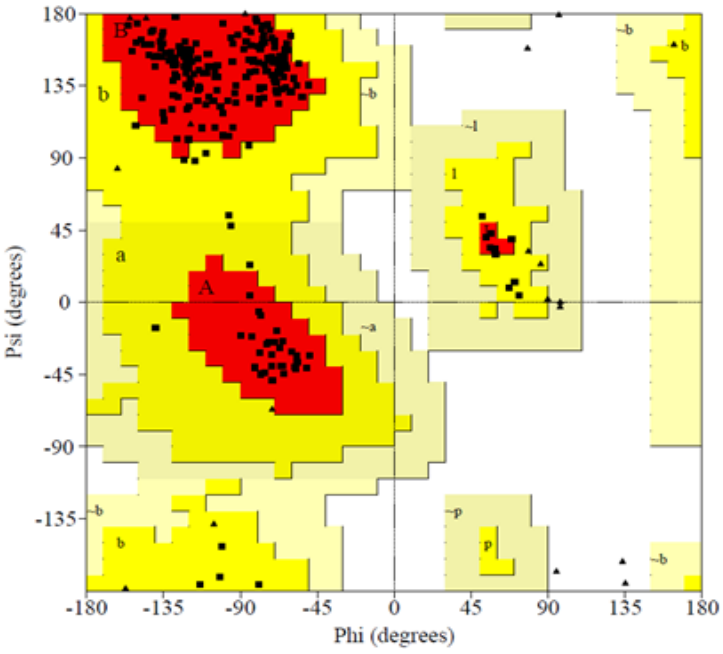

Fig. S8B. Validation of the D2D3M3M4 chimera model. The chimera D2D3M3M4 constructed using the template structures of DAF and MCP was evaluated using the PROCHECK program. The generated Ramachandran plots for D2D3M3M4 chimera and multi-4 mutant showing their phi-psi profiles are shown in (i) and (ii) respectively.

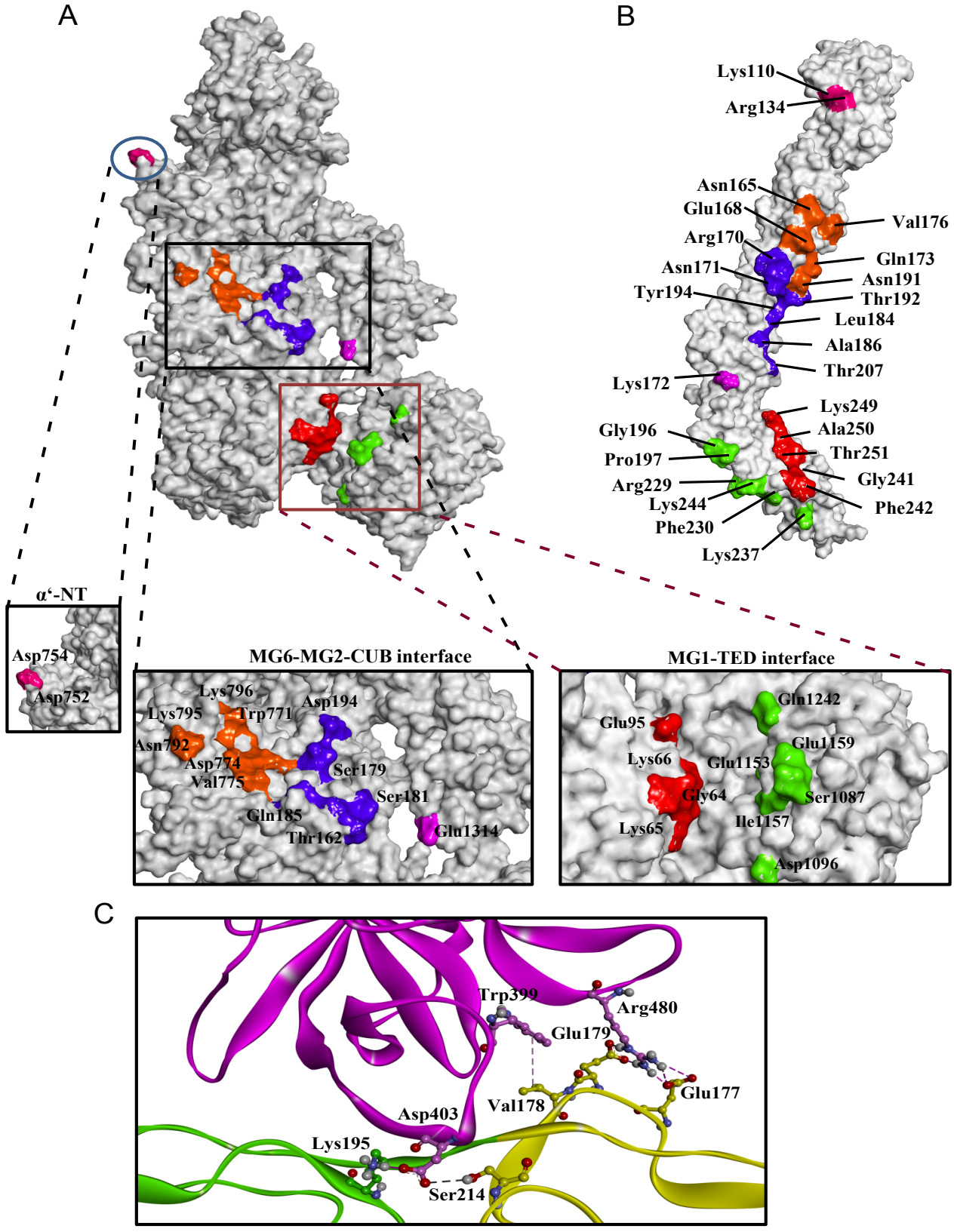

Fig. S9. Mapping of interaction of multi-4 mutant with C3b and FI in C3b-multi-4 mutant-FI complex. (A) DAF (D2-D3) as well MCP domains (M3-M4) of multi-4 mutant show interaction with C3b. The zoomed views show interacting residues in α'-NT (Pink), MG6 (Orange), MG2 (blue), CUB (magenta), MG1 (red), and TED (green) domains. B) C3b interacting residues of multi-4 mutant. The coloring of the C3b interacting residues of multi-4 mutant is according to the color of the C3b domains with which it interacts. C) Interactions of the M3 domain residues with FI. Glu177 and Glu179 show strong charge interactions with Arg480 of FI. Also, Lys195 show charge interaction with Asp403 of FI which is helped by its hydrogen bond with Ser214 of the M3 domain. V178 display a pi-alkyl bond with Trp399 of FI.

Fig.S10A

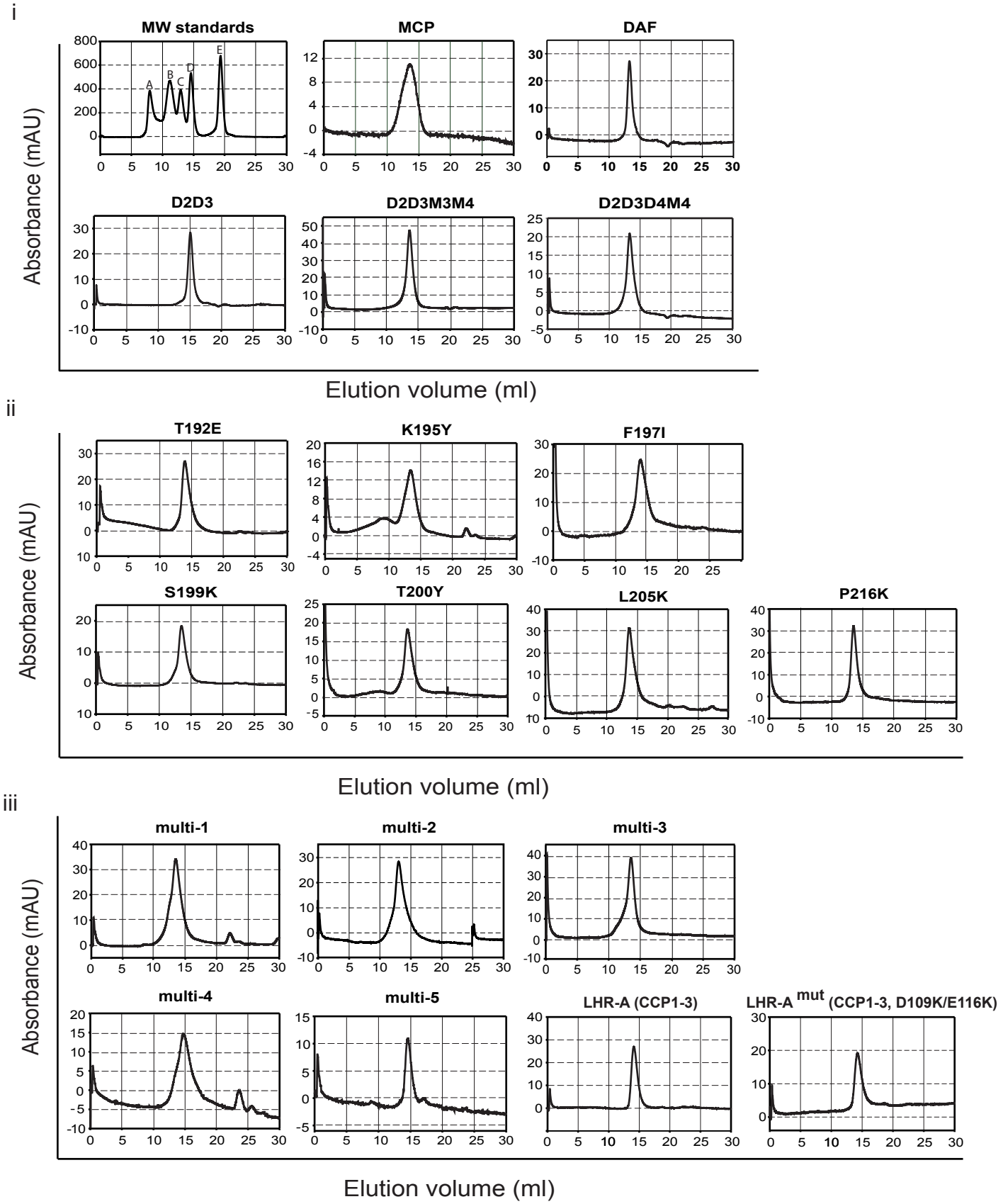

Fig. S10A. Size exclusion chromatography analysis of DAF, MCP, the DAF-MCP chimeras D2D3M3M4 and D2D3D4M4, and the single and multiresidue mutants of D2D3M3M4. (i) DAF, MCP and the DAF-MCP chimeras. (ii) Single residue mutants of D2D3M3M4. (iii) Multi-residue mutants of D2D3M3M4 - multi-1, multi-2, multi-3, multi-4 and multi-5 along with CR1 LHR-A (CCP1-3) and it's double mutant CR1 LHR-A (CCP1-3 D109N/E116K). Proteins were loaded onto Superose-12 column (GE Healthcare Life Sciences) pre-equilibrated with PBS (pH 7.4). The gel filtration standards (Bio-Rad) used were: a, Thyroglobulin (670,000 Da); b, Gamma globulin (158,000 Da); c, Ovalbumin (44,000 Da); d, Myoglobin (17,000 Da); e, Vitamin B-12 (1,350 Da).

Fig.S10B

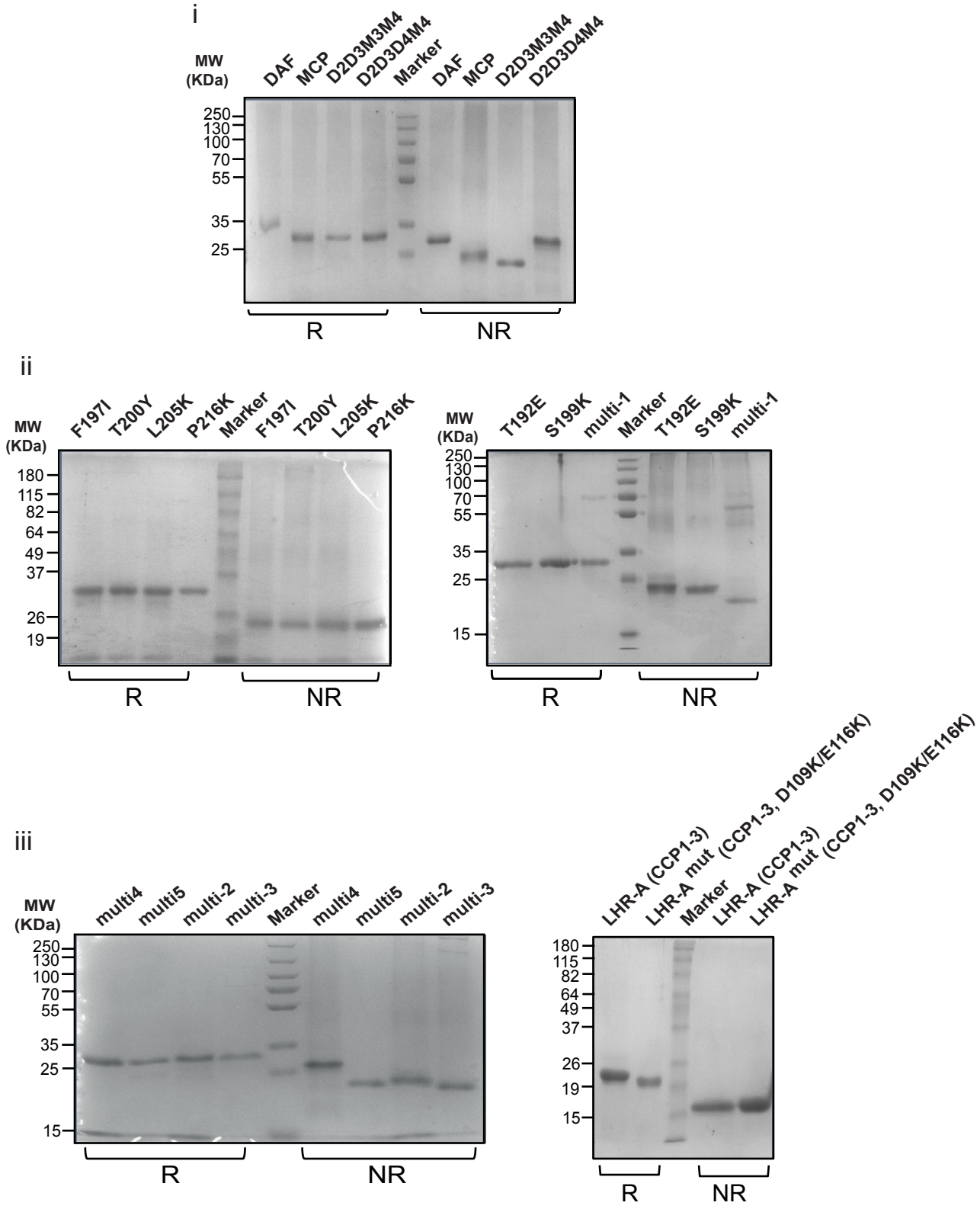

Fig. S10B. SDS-PAGE analysis of purified DAF, MCP, the DAF-MCP chimeras D2D3M3M4 and D2D3D4M4, and the single and multiresidue mutants of D2D3M3M4. (i) DAF, MCP and the DAF-MCP chimeras. (ii) Single and multiresidue (multi-1) mutants of D2D3M3M4. (iii) multi-residue mutants of D2D3M3M4 (iv) CR1 LHR-A CCP(1-3) and its double mutant CR1 LHR-A (CCP1-3 D109N/E116K). All the proteins were run on 9% SDS-PAGE under reducing (R) and non-reducing (NR) conditions and were stained with Coomassie blue.

REFERENCES

1. Ahmad M, Raut S, Pyaram K, Kamble A, Mullick J, Sahu A (2010) Domain swapping reveals complement control protein modules critical for imparting cofactor and decay-accelerating activities in vaccinia virus complement control protein. *J Immunol* **185:**6128-6137.

2. Mullick J, Bernet J, Panse Y, Hallihosur S, Singh AK, Sahu A (2005) Identification of complement regulatory domains in vaccinia virus complement control protein. *J Virol* **79:**12382-12393.

3. Ip WK, Chan KH, Law HK, Tso GH, Kong EK, Wong WH, To YF, Yung RW, Chow EY, Au KL *et al.* (2005) Mannose-binding lectin in severe acute respiratory syndrome coronavirus infection. *J Infect Dis* **191:**1697-1704.

4. Pyaram K, Kieslich CA, Yadav VN, Morikis D, Sahu A (2010) Influence of electrostatics on the complement regulatory functions of Kaposica, the complement inhibitor of Kaposi's sarcoma-associated herpesvirus. *J Immunol* **184:**1956-1967.

5. Yadav VN, Pyaram K, Mullick J, Sahu A (2008) Identification of hot spots in the variola virus complement inhibitor (SPICE) for human complement regulation. *J Virol* **82:**3283-3294.

6. Pan Q, Ebanks RO, Isenman DE (2000) Two clusters of acidic amino acids near the NH2 terminus of complement component C4 alpha'-chain are important for C2 binding. *J Immunol* **165:**2518-2527.

7. Okroj M, Mark L, Stokowska A, Wong SW, Rose N, Blackbourn DJ, Villoutreix BO, Spiller OB, Blom AM (2009) Characterization of the complement inhibitory function of Rhesus rhadinovirus complement control protein (RCP). *J Biol Chem* **284:**505-514.

8. Liszewski MK, Leung MK, Hauhart R, Buller RM, Bertram P, Wang X, Rosengard AM, Kotwal GJ, Atkinson JP (2006) Structure and regulatory profile of the monkeypox inhibitor of complement: comparison to homologs in vaccinia and variola and evidence for dimer formation. *J Immunol* **176:**3725-3734.

9. Seya T, Holers VM, Atkinson JP (1985) Purification and functional analysis of the polymorphic variants of the C3b/C4b receptor (CR1) and comparison with H, C4b-binding protein (C4bp), and decay accelerating factor (DAF). *J Immunol* **135:**2661-2667.

10. Reza MJ, Kamble A, Ahmad M, Krishnasastry MV, Sahu A (2013) Dissection of functional sites in herpesvirus saimiri complement control protein homolog. *J Virol* **87:**282-295.

11. Sahu A, Isaacs SN, Soulika AM, Lambris JD (1998) Interaction of vaccinia virus complement control protein with human complement proteins: factor I-mediated degradation of C3b to $iC3b_1$ inactivates the alternative complement pathway. *J Immunol* **160:**5596-5604.

12. Mullick J, Singh AK, Panse Y, Yadav V, Bernet J, Sahu A (2005) Identification of functional domains in kaposica, the complement control protein homolog of Kaposi's sarcoma-associated herpesvirus (human herpesvirus-8). *J Virol* **79:**5850-5856.

13. Kumar J, Yadav VN, Phulera S, Kamble A, Gautam AK, Panwar HS, Sahu A (2017) Species specificity of vaccinia virus complement control protein towards bovine classical pathway is governed primarily by direct interaction of its acidic residues with factor I. *J Virol*.

14. Sali A, Potterton L, Yuan F, van Vlijmen H, Karplus M (1995) Evaluation of comparative protein modeling by MODELLER. *Proteins* **23:**318-326.

15. Humphrey W, Dalke A, Schulten K (1996) VMD: visual molecular dynamics. *J Mol Graph* **14:**33-38.

16. Laskowski RA, MacArthur MW, Moss DS, Thornton JM (1993) PROCHECK: a program to check the stereochemical quality of protein structures . *J Appl Cryst* **26:**283-291.

17. Wiederstein M, Sippl MJ (2007) ProSA-web: interactive web service for the recognition of errors in three-dimensional structures of proteins. *Nucleic Acids Res* **35:**W407-W410.

18. Pettersen EF, Goddard TD, Huang CC, Couch GS, Greenblatt DM, Meng EC, Ferrin TE (2004) UCSF Chimera--a visualization system for exploratory research and analysis. *J Comput Chem* **25:**1605-1612.

19. Kaminski GA, Friesner RA, Tirado-Rives J, Jorgensen WL (2001) Evaluation and Reparametrization of the OPLS-AA Force Field for Proteins via Comparison with Accurate Quantum Chemical Calculations on Peptides. *J Phys Chem* **105:**6474-6487.

20. Pronk S, Pall S, Schulz R, Larsson P, Bjelkmar P, Apostolov R, Shirts MR, Smith JC, Kasson PM, van der SD *et al.* (2013) GROMACS 4.5: a high-throughput and highly parallel open source molecular simulation toolkit. *Bioinformatics* **29:**845-854.

21. Hess B (2008) P-LINCS: a parallel linear constraint solver for molecular simulation. *J Chem Theory Comput* **4:**116-122.

22. Essmann U, Perera L, Berkowitz ML, Darden T, Lee H, Pedersen LG (1995) A smooth particle mesh Ewald method. *J Chem Phys* **103:**8577.

23. Daura X, Gademann K, Jaun B, Seebach D, Gunsteren W, Mark A (1999) Peptide folding: when simulation meets experiment. *Angew Chem* **38:**236-240.